

Vestigial chiral and charge orders from bidirectional spin-density waves: Application to the iron-based superconductors

R. M. Fernandes,¹ S. A. Kivelson,² and E. Berg³

¹*School of Physics and Astronomy, University of Minnesota, Minneapolis 55455, USA*

²*Department of Physics, Stanford University, Stanford, California 94305, USA*

³*Department of Condensed Matter Physics, Weizmann Institute of Science, Rehovot, Israel 76100*

(Received 9 July 2015; revised manuscript received 15 December 2015; published 19 January 2016)

Recent experiments in optimally hole-doped iron arsenides have revealed a novel magnetically ordered ground state that preserves tetragonal symmetry, consistent with either a charge-spin density wave (CSDW), which displays a nonuniform magnetization, or a spin-vortex crystal (SVC), which displays a noncollinear magnetization. Here we show that, similarly to the partial melting of the usual stripe antiferromagnet into a nematic phase, either of these phases can also melt in two stages. As a result, intermediate paramagnetic phases with vestigial order appears: a checkerboard charge density wave for the CSDW ground state, characterized by an Ising-like order parameter, and a remarkable spin-vorticity density wave for the SVC ground state—a triplet d -density wave characterized by a vector chiral order parameter. We propose experimentally detectable signatures of these phases, show that their fluctuations can enhance the superconducting transition temperature, and discuss their relevance to other correlated materials.

DOI: [10.1103/PhysRevB.93.014511](https://doi.org/10.1103/PhysRevB.93.014511)

I. INTRODUCTION

One of the hallmarks of the superconducting state of the iron-based materials [1] is its typical proximity to a stripe magnetically ordered state, with spins aligned parallel to each other along one in-plane direction and antiparallel along the other [see Fig. 1(a)] [2]. As a result, this stripe state breaks two distinct symmetries of the high-temperature paramagnetic-tetragonal state: a continuous spin-rotational $O(3)$ symmetry and an Ising-like Z_2 symmetry related to the equivalence of the x and y directions [3–9]. Magnetic fluctuations present in the paramagnetic state can cause these two symmetries to be broken at different temperatures, giving rise to an intermediate nematic phase that preserves the spin-rotational $O(3)$ symmetry but, as a “vestigial” of the stripe order [10], breaks the tetragonal Z_2 symmetry [11]. Indeed, in the phase diagrams of most iron-based superconductors, the magnetic transition line is closely followed by the structural/nematic one at slightly higher temperatures. The corresponding nematic degrees of freedom impact not only the normal state electronic properties [12–21] but also the onset and gap structure of the superconducting state [22–24].

Recently, experiments in the hole-doped pnictides $\text{Ba}(\text{Fe}_{1-x}\text{Mn}_x)_2\text{As}_2$ [25], $(\text{Ba}_{1-x}\text{Na}_x)\text{Fe}_2\text{As}_2$ [26], and $(\text{Ba}_{1-x}\text{K}_x)\text{Fe}_2\text{As}_2$ [27] have revealed another type of magnetically ordered state that does not break the tetragonal Z_2 symmetry of the lattice. Neutron scattering experiments [25,26] showed that its magnetic Bragg peaks are at the same momenta as in the stripe magnetic phase—namely, $\mathbf{Q}_1 = (\pi, 0)$ and $\mathbf{Q}_2 = (0, \pi)$ in the Fe-only Brillouin zone. Consequently, it has been proposed [26,28–31] that the tetragonal magnetic state is the realization of one of two possible biaxial (i.e., double- \mathbf{Q}) magnetic orders [6,32–34]. One possibility is a “charge-spin density wave” (CSDW), displaying a nonuniform magnetization which vanishes at the even lattice sites and is staggered along the odd lattice sites [Fig. 1(b)]. The other option is a “spin-vortex crystal” (SVC), in which the magnetization is noncollinear (but coplanar) and forms spin vortices staggered across the plaquettes [Fig. 1(c)]. Both

CSDW and SVC phases are tetragonal, but have a unit cell four times larger than the paramagnetic phase. Interestingly, in $(\text{Ba}_{1-x}\text{Na}_x)\text{Fe}_2\text{As}_2$ and $(\text{Ba}_{1-x}\text{K}_x)\text{Fe}_2\text{As}_2$, the tetragonal magnetic state is observed very close to optimal doping [26,27], where superconductivity displays its highest transition temperature. Therefore, understanding the properties of these biaxial tetragonal magnetic phases is important to assess their relevance for the superconductivity.

In this paper, we show that both the CSDW and the SVC magnetic phases support composite order parameters that can condense at temperatures above the onset of magnetic order, and whose fluctuations can help enhancing T_c . As with the nematic phase, these partially ordered phases are paramagnetic, i.e., fluctuations restore the time-reversal symmetry that is broken in the ground state. In contrast to the nematic phase, however, they preserve the point group symmetry of the lattice, but break other symmetries, including translational symmetry [35]. In particular, upon melting the CSDW phase, we find a vestigial *Ising-like* charge-density wave (CDW) phase with ordering vector $\mathbf{Q}_1 + \mathbf{Q}_2 = (\pi, \pi)$, in which the previously magnetized sites acquire a different charge than the previously nonmagnetized sites. On the other hand, upon melting the SVC ground state, we find a vestigial phase that retains memory of the preferred plane of magnetization (in spin space), and of the staggering of the spin vortices across the plaquettes. This spin-vorticity density wave (SVDW) is a triplet d -density wave characterized by a *vector chiral* order parameter, which is manifested as a spin-current density wave with modulation $\mathbf{Q}_1 + \mathbf{Q}_2 = (\pi, \pi)$. Besides shedding light on the magnetism of hole-doped iron pnictides, our results provide a microscopic mechanism for the formation of d -density waves, which have also been proposed in cuprates [36] and heavy fermions [37].

The paper is organized as follows: in Sec. II we present the theoretical model that gives rise to the vestigial CDW and SVDW orders. Section III discusses the implications of these vestigial orders for both the normal state and superconducting state properties. Concluding remarks are presented in Sec. IV. To make the paper transparent and accessible, all formal details are presented in Appendices. Appendix A contains

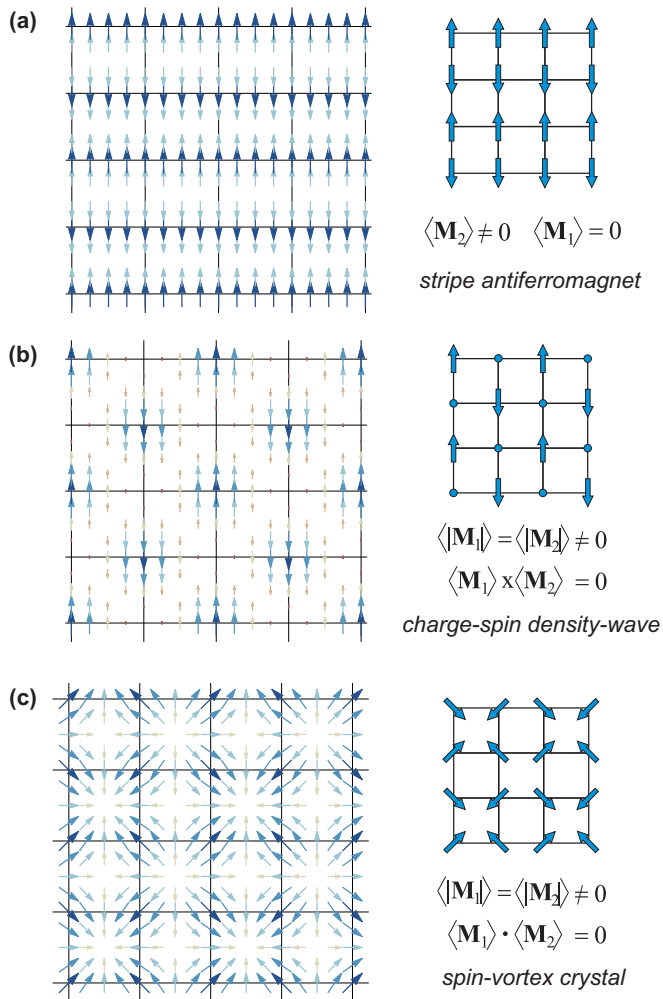


FIG. 1. Magnetic ground states of the iron pnictides: (a) stripe antiferromagnet, (b) charge-spin density wave (CSDW), and (c) spin-vortex crystal (SVC). The first is orthorhombic with a doubled unit cell; the latter two remain tetragonal but with a quadrupled unit cell. \mathbf{M}_1 and \mathbf{M}_2 are the magnetic order parameters corresponding to the ordering vectors $\mathbf{Q}_1 = (\pi, 0)$ and $\mathbf{Q}_2 = (0, \pi)$. The left panels are the actual spin density-wave patterns in real space, whereas the right panels are schematic representations focusing on the magnetization at the lattice sites.

the derivation of the saddle-point equations that give the phase diagram of the SVDW phase discussed in Sec. II. In Appendix B we derive microscopically the free energy discussed in Sec. III. Finally, Appendix C presents the derivation of the effective pairing interactions promoted by CDW and SVDW fluctuations discussed in Sec. III.

II. THEORETICAL MODEL FOR THE VESTIGIAL PHASES

A. Effective action

We define two magnetic order parameters, \mathbf{M}_1 and \mathbf{M}_2 , associated with the two ordering vectors $\mathbf{Q}_1 = (\pi, 0)$ and $\mathbf{Q}_2 = (0, \pi)$, respectively. Thus, the local spin is given by $\mathbf{S}(\mathbf{r}) = \sum_i \mathbf{M}_i e^{i\mathbf{Q}_i \cdot \mathbf{r}}$. As discussed in Refs. [6,8,28–30,32–34], the most general lowest order action that respects the tetragonal

and spin-rotational symmetries is given by

$$\mathcal{S}[\mathbf{M}_i] = \int_q \chi_q^{-1} (\mathbf{M}_1^2 + \mathbf{M}_2^2) + \frac{u}{2} \int_x (\mathbf{M}_1^2 + \mathbf{M}_2^2)^2 - \frac{g}{2} \int_x (\mathbf{M}_1^2 - \mathbf{M}_2^2)^2 + 2w \int_x (\mathbf{M}_1 \cdot \mathbf{M}_2)^2. \quad (1)$$

For simplicity, we will consider the finite temperature problem, but the same conclusions can be extended to the quantum case. Here, $\int_q \equiv \int \frac{d^d q}{(2\pi)^d}$ and $\int_x \equiv \int d^d x$ where \mathbf{q} is the momentum and \mathbf{x} is the position. In the neighborhood of a finite T magnetic transition, and for a quasi-two-dimensional (quasi-2D) system, we can use the small q expansion $\chi_q^{-1} \approx r_0 + q_{\parallel}^2 + J_z \sin^2 \frac{q_z}{2}$, where r_0 is the distance to the mean-field magnetic critical point.

The quartic coefficients u, g, w determine the nature of the magnetic ground state. These are, in turn, sensitive to microscopic considerations. The localized J_1 - J_2 model favors positive g and w [38]. On the other hand, itinerant approaches (at weak and strong coupling) have found parameter regimes in which g and w can be either positive or negative [6,8,28–30,32–34,39]. For $g > \max(0, -w)$, the energy is minimized by the stripe state shown in Fig. 1(a), in which either $\langle \mathbf{M}_1 \rangle = 0$ or $\langle \mathbf{M}_2 \rangle = 0$. Thus, in addition to breaking the $O(3)$ spin-rotational symmetry, the magnetic ground state spontaneously breaks a Z_2 symmetry by selecting one of the two order parameters to be nonzero. Since \mathbf{M}_1 and \mathbf{M}_2 are related by a 90° rotation, once this Z_2 symmetry is broken the tetragonal symmetry of the system is lowered to orthorhombic [see Fig. 2(a)]. A composite Ising-nematic order parameter, living on the bonds of the lattice, can be identified by performing a Hubbard-Stratonovich transformation on the quartic term with coefficient g , yielding $\langle \varphi_{\text{nem}} \rangle = g \langle \mathbf{M}_1^2 - \mathbf{M}_2^2 \rangle$. Because Z_2 is a discrete symmetry, while spin-rotational $O(3)$ is a continuous symmetry, a strongly anisotropic three-dimensional (3D) system will generically display a vestigial paramagnetic nematic phase where $\langle \mathbf{M}_i \rangle = 0$ but $\langle \varphi_{\text{nem}} \rangle \neq 0$ [3,8,40].

For $g < \max(0, -w)$, the ground state of Eq. (1) is no longer a uniaxial magnetic stripe state, but a biaxial magnetic state with $|\langle \mathbf{M}_1 \rangle| = |\langle \mathbf{M}_2 \rangle|$ that preserves tetragonal symmetry. If $w < 0$, the energy is minimized by $\langle \mathbf{M}_1 \rangle \parallel \langle \mathbf{M}_2 \rangle$, which in terms of the local spin configuration $\mathbf{S}(\mathbf{r})$ corresponds to a nonuniform state as depicted in Fig. 1(b). We identify this state as a charge-spin density wave (CSDW). On the other hand, if $w > 0$, the energy minimization gives $\langle \mathbf{M}_1 \rangle \perp \langle \mathbf{M}_2 \rangle$, corresponding to a noncollinear, coplanar spin configuration [see Fig. 1(c)]. This state is identified as a spin-vortex crystal (SVC). We now discuss whether these tetragonal magnetic phases can melt in a two-stage process, giving rise to vestigial orders akin to the nematic phase.

B. Charge-density wave

Consider the CSDW state: Once the magnetization direction is chosen by spontaneous breaking of the $O(3)$ spin-rotational symmetry, there remains a fourfold degeneracy corresponding to whether \mathbf{M}_1 and \mathbf{M}_2 are parallel or antiparallel to the chosen direction. As is apparent in Fig. 1(b), this corresponds to the breaking of translational symmetry, leading to a four-site unit cell. Notice, however,

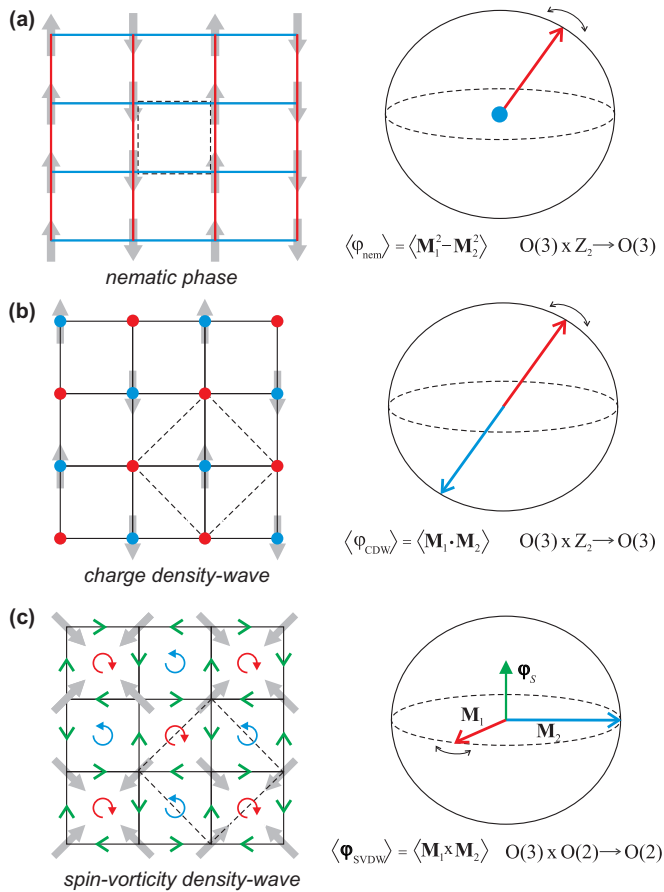


FIG. 2. The vestigial composite states associated with (a) the stripe antiferromagnet, (b) the CSDW state, and (c) the SVC state. The real-space spins (in gray) and the magnetic order parameters in spin space (red and blue arrows, representing \mathbf{M}_1 and \mathbf{M}_2 , respectively) should be understood as fluctuating, i.e., $\langle \mathbf{M}_i \rangle = 0$ in all cases. In (a), the vestigial state is nematic (unequal blue and red bonds), associated with selecting between \mathbf{M}_1 and \mathbf{M}_2 fluctuations in spin space. The original unit cell is shown as a dashed square. In (b), the vestigial state breaks translational symmetry via a checkerboard charge density wave (unequal blue and red sites). \mathbf{M}_1 and \mathbf{M}_2 are locked to be collinear in spin space. In (c), the vestigial spin-vorticity density-wave state breaks inversion and translational symmetries via a staggered pattern of spin vortices in the center of the plaquettes (unequal blue and red plaquettes). The corresponding spin-current pattern is shown by the green arrows. Because \mathbf{M}_1 and \mathbf{M}_2 are locked to be orthogonal in spin space, the residual spin-rotational symmetry is $O(2)$ instead of $O(3)$. Both (b) and (c) preserve tetragonal symmetry, as shown by the dashed-line unit cell.

that the product of a translation by the vector $\hat{x} + \hat{y}$ followed by time reversal is preserved. Thus, there is an essential Z_2 symmetry that interchanges the magnetic and nonmagnetic sublattices of the CSDW state.

The order parameter field for this Z_2 symmetry is obtained via a Hubbard-Stratonovich transformation on the quartic term with coefficient $2w$ in Eq. (1), $\langle \varphi_{\text{CDW}} \rangle = 2|w|\langle \mathbf{M}_1 \cdot \mathbf{M}_2 \rangle$. Clearly, φ_{CDW} is a scalar that carries momentum $\mathbf{Q}_1 + \mathbf{Q}_2 = (\pi, \pi)$, i.e., the condensed phase is a CDW that doubles the unit cell, but leaves time-reversal and the tetragonal symmetry of the lattice intact [see Fig. 2(b)]. Thus, in real space, the

CDW order parameter lives on the lattice sites. The fact that the unit cell decreases from four to two sites upon going from the CSDW to the CDW phase is due to the restoration of time-reversal symmetry, which implies the restoration of the translational symmetry by $\hat{x} + \hat{y}$. A simple change of variables in Eq. (1), $\mathbf{M}_1 \rightarrow 2^{-1/2}[\mathbf{M}_1 + \mathbf{M}_2]$ and $\mathbf{M}_1 \rightarrow 2^{-1/2}[\mathbf{M}_1 - \mathbf{M}_2]$, interchanges the identities of the two scalar orders, $\varphi_{\text{nem}} \leftrightarrow \varphi_{\text{CDW}}$, but leaves the form of S unchanged albeit with $(g, w) \rightarrow -(w, g)$. Thus, the properties of the CDW phase are akin to those of the Ising-nematic phase—in particular, a quasi-2D system will again display for a range of intermediate temperatures a phase with $\langle \mathbf{M}_i \rangle = 0$ but $\langle \varphi_{\text{CDW}} \rangle \neq 0$.

C. Spin-vorticity density wave

Consider now the SVC state, characterized by two equal magnitude orthogonal vectors \mathbf{M}_1 and \mathbf{M}_2 . Upon fixing the direction of \mathbf{M}_1 , which breaks the $O(3)$ spin-rotational symmetry, there remains an additional $O(2)$ symmetry related to choosing \mathbf{M}_2 in any direction along the plane perpendicular to \mathbf{M}_1 [41]. Thus, the SVC phase can be completely characterized by a pseudovector order parameter φ_{SVDW} that specifies the ordering plane which contains \mathbf{M}_1 and \mathbf{M}_2 , and also by the orientation of \mathbf{M}_1 within that plane. φ_{SVDW} is obtained via a Hubbard-Stratonovich transformation of the quartic term $w(\mathbf{M}_1 \cdot \mathbf{M}_2)^2 \rightarrow -w(\mathbf{M}_1 \times \mathbf{M}_2)^2$ in Eq. (1), yielding $\langle \varphi_{\text{SVDW}} \rangle = 2w\langle \mathbf{M}_1 \times \mathbf{M}_2 \rangle$, which can be identified as a vector chirality [42–44]. Thus, upon approaching the SVC phase from high-temperatures or by melting it, there can be an intermediate state where $\langle \varphi_{\text{SVDW}} \rangle \neq 0$ but the orientation of \mathbf{M}_1 is not fixed, $\langle \mathbf{M}_1 \rangle = 0$. This chiral paramagnetic state preserves time-reversal symmetry and retains the memory of the staggering pattern of spin vortices along the plaquettes in the SVC phase, and is therefore called a spin-vorticity density wave (SVDW) [43]. Note that the vector chirality order parameter produces an emergent Dzyaloshinskii-Moriya coupling $\varphi_{\text{SVDW}} \cdot (\mathbf{M}_1 \times \mathbf{M}_2)$ relating the translational symmetry breaking to a preferred “handedness” in spin space. In the SVDW state, not only is the translational symmetry lowered by the doubling of the unit cell [since φ_{SVDW} carries momentum $\mathbf{Q}_1 + \mathbf{Q}_2 = (\pi, \pi)$], but also the soft spin fluctuations near the magnetic transition are constrained to lie in the plane defined by φ_{SVDW} [see Fig. 2(c)].

Because φ_{SVDW} breaks a continuous $O(3)$ symmetry, there are two Goldstone modes in the SVDW phase. Consequently, in contrast to the Ising-nematic cases, the Mermin-Wagner theorem does not ensure the existence of the SVDW phase even in the two-dimensional limit. To investigate whether $\langle \varphi_{\text{SVDW}} \rangle \neq 0$ while $\langle \mathbf{M}_1 \rangle = 0$ is possible, we calculated the phase diagram for a magnetic SVC ground state treating the action in Eq. (1) in the saddle point approximation (see Appendix A). We find that for a strongly anisotropic system, i.e., $J_z \ll w$, there is a wide range of values of u/w for which there are two transitions, with an intermediate SVDW phase and a low-temperature SVC phase (see Fig. 3). However, in this approximation, the transition to the SVDW phase is always first order.

Spin rotational symmetry is not an exact symmetry of nature, and indeed most iron pnictides display a sizable spin anisotropy [45–47]. Because the ordered moments tend to point parallel to the FeAs plane, the most significant effects

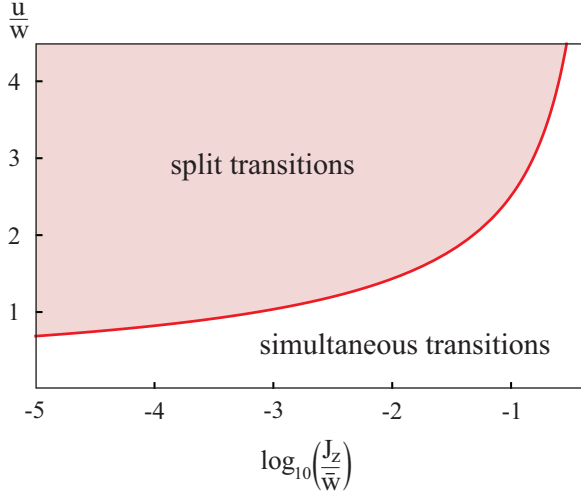


FIG. 3. Phase diagram, within the saddle-point approximation, of the coupled SVDW paramagnetic and SVC magnetic transitions. In the shaded area, where the out-of-plane anisotropy is strong, the two transitions are split. The tuning parameters are the Ginzburg-Landau coefficients u and w [see Eq. (1)] and the magnetic coupling between layers J_z . The parameter \bar{w} is given by $w = T_{N,0}w/2\pi$, as discussed in Appendix B.

of spin-orbit coupling can be captured phenomenologically in Eq. (1) by including an easy-plane anisotropy term $\kappa(M_{1,z}^2 + M_{2,z}^2)$ with coupling constant $\kappa > 0$ [48]. The spin rotational symmetry is thus reduced to $O(2)$ and the SVDW chiral order parameter becomes the pseudoscalar $\varphi_{\text{SVDW}} = 2w(\mathbf{M}_1 \times \mathbf{M}_2) \cdot \hat{\mathbf{z}}$, which only breaks a discrete chiral Z_2 symmetry. For such an $O(2) \times Z_2$ model, it is known from both numerical and analytical investigations that in two dimensions the Z_2 symmetry is broken at higher temperatures than the Kosterlitz-Thouless transition of the $O(2)$ order parameter [49,50], i.e., there is no doubt that there is a vestigial chiral SVDW phase. The extent to which the spin anisotropy is quantitatively significant depends on the (currently unknown) value of the ratio $\kappa/(T_{\text{SVDW}} - T_{\text{SVC}})$.

III. MICROSCOPIC IMPLICATIONS OF THE VESTIGIAL ORDERS

A. Normal-state manifestations

To discuss the experimental manifestations of the vestigial CDW and SVDW states, we investigate their coupling to the low-energy electronic states of the pnictides. We consider a three-band model [6,8] with a circular hole pocket $\xi_{h,\mathbf{k}}$ at the center of the Brillouin zone, and two elliptical electron pockets $\xi_{e_1,\mathbf{k}+\mathbf{Q}_1}$ and $\xi_{e_2,\mathbf{k}+\mathbf{Q}_2}$ centered at momenta $\mathbf{Q}_1 = (\pi, 0)$ and $\mathbf{Q}_2 = (0, \pi)$, respectively (see Fig. 4). The magnetic order parameters couple to these electronic states via $\sum_{\mathbf{k},\alpha\beta} \mathbf{M}_i \cdot \sigma_{\alpha\beta} (c_{h,\mathbf{k}\alpha}^\dagger c_{e_i,\mathbf{k}\beta} + \text{H.c.})$, where the operator $c_{a,\mathbf{k}\alpha}$ annihilates an electron in band a with momentum \mathbf{k} (measured with respect to the center of the pocket) and spin α , and $\sigma_{\alpha\beta}$ are Pauli matrices. We further introduce magnetic Δ_S and charge Δ_C order parameters with ordering vector $\mathbf{Q}_1 + \mathbf{Q}_2 = (\pi, \pi)$,

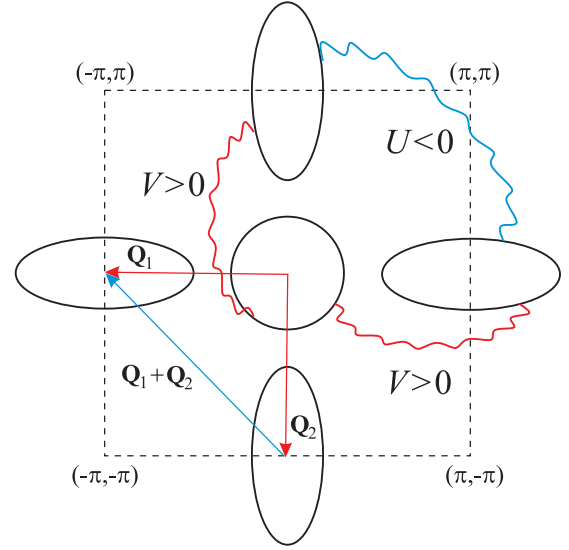


FIG. 4. Schematic Fermi surface of the iron pnictides, with a central hole pocket and elliptical electron pockets. The wavy lines represent the inter-pocket pairing interactions generated by the magnetic fluctuations (repulsive $V > 0$) and by fluctuations of the vestigial CDW and SVDW states (attractive $U < 0$).

which couple to the electronic states via

$$\begin{aligned} \mathcal{H}_S &= \sum_{\mathbf{k},\alpha\beta} [\Delta_S \cdot \sigma_{\alpha\beta} c_{e_2,\mathbf{k}\alpha}^\dagger c_{e_1,\mathbf{k}\beta} + \text{H.c.}], \\ \mathcal{H}_C &= \sum_{\mathbf{k},\alpha\beta} [\Delta_C \delta_{\alpha\beta} c_{e_2,\mathbf{k}\alpha}^\dagger c_{e_1,\mathbf{k}\beta} + \text{H.c.}]. \end{aligned} \quad (2)$$

Here these fields have real and imaginary parts, $\Delta_S = \Delta'_S + i\Delta''_S$ and $\Delta_C = \Delta'_C + i\Delta''_C$, where the real parts correspond to conventional spin-density wave (SDW) or CDW orders, while the imaginary parts corresponds to spin or charge current orders. By integrating out the electronic degrees of freedom, we obtain the coupling between \mathbf{M}_i and Δ_S, Δ_C to the lowest order in the action (see Appendix B):

$$\delta\mathcal{S}_{\text{eff}} = \lambda[\Delta''_S \cdot (\mathbf{M}_1 \times \mathbf{M}_2) - \Delta'_C(\mathbf{M}_1 \cdot \mathbf{M}_2)], \quad (3)$$

with the coefficient $\lambda = 4 \int_k G_{h,k} G_{e_1,k} G_{e_2,k}$, where $G_{a,k}^{-1} = i\omega_n - \xi_{a,\mathbf{k}}$ is the corresponding noninteracting Green's function. As expected, the Ising-like order parameter $\varphi_{\text{CDW}} \propto \mathbf{M}_1 \cdot \mathbf{M}_2$ induces a checkerboardlike charge order [see Fig. 2(b)]. On the other hand, the SVDW order parameter $\varphi_{\text{SVDW}} \propto \mathbf{M}_1 \times \mathbf{M}_2$ is manifested as a spin-current density wave with propagation vector (π, π) , i.e., a spin current polarized parallel to φ_{SVDW} and propagating along the bonds of the lattice in a staggered pattern across the square plaquettes [see Fig. 2(c)]. Thus, the SVDW corresponds to a triplet d -density wave [36].

Note that probing the CDW via x rays may be difficult, since the hybridization between Fe and As/Se doubles the unit cell of the Fe-only square lattice, making (π, π) a lattice Bragg peak. While the real CDW could in principle be detected experimentally by a probe sensitive to the local charge on the Fe sites, such as scanning tunneling microscopy (STM), detecting a spin-current density wave would be rather challenging. Alternatively, one can consider the effects of a Zeeman field \mathbf{H} . Despite not coupling to φ_{nem} , we find that it

TABLE I. Magnetic ground states of the pnictides and their corresponding vestigial states. \mathbf{M}_1 and \mathbf{M}_2 are the magnetic order parameters corresponding to the ordering vectors $\mathbf{Q}_1 = (\pi, 0)$ and $\mathbf{Q}_2 = (0, \pi)$.

Magnetic ground state	Vestigial state	Broken symmetry	Real space pattern	Physical manifestation
Stripe: $\langle \mathbf{M}_2 \rangle$ or $\langle \mathbf{M}_1 \rangle = 0$	Nematic: $\langle \mathbf{M}_1^2 - \mathbf{M}_2^2 \rangle \neq 0$	Rotational (tetragonal)	Unequal bonds	Orthorhombic distortion
CSDW: $\langle \mathbf{M}_1 \rangle \parallel \langle \mathbf{M}_2 \rangle$	CDW: $\langle \mathbf{M}_1 \cdot \mathbf{M}_2 \rangle \neq 0$	Translational	Unequal sites	Charge density wave
SVC: $\langle \mathbf{M}_1 \rangle \perp \langle \mathbf{M}_2 \rangle$	SVDW: $\langle \mathbf{M}_1 \times \mathbf{M}_2 \rangle \neq \mathbf{0}$	Translational + inversion	Unequal plaquettes	Spin-current density wave

couples to both φ_{CDW} and φ_{SVDW} in the action via the terms $\gamma \Delta_C'' \mathbf{H} \cdot (\mathbf{M}_1 \times \mathbf{M}_2)$ and $\gamma (\mathbf{H} \cdot \Delta_S') (\mathbf{M}_1 \cdot \mathbf{M}_2)$, with the same Ginzburg-Landau coefficient γ . Therefore, in the presence of a magnetic field, a pattern of staggering orbital currents (i.e., a singlet d -density wave [36]) appears in the SVDW state, which can in principle be detected by NMR. Table I summarizes the magnetic ground states of the pnictides along their vestigial paramagnetic states.

B. Impact on the superconducting state

Fluctuations of the SVDW and CDW states arise from four-spin correlations, and are complementary to the magnetic fluctuations that arise from two-spin correlations. An important issue is whether these fluctuation modes promote compatible superconducting states. Because the magnetic fluctuations are peaked at momenta $\mathbf{Q}_1 = (\pi, 0)$ and $\mathbf{Q}_2 = (0, \pi)$, they promote a *repulsive* interpocket interaction $V > 0$ between the hole and the electron pockets (see Fig. 4). Solution of the corresponding linearized gap equations yields the so-called s^{+-} state, where the gap functions have different signs in the electron and in the hole pockets [51]. The transition temperature is given by $T_c \propto \exp(-\frac{1}{\Lambda_0})$, with $\Lambda_0 = \sqrt{2N_h N_e} V$, and N_a denoting the density of states of band a .

The SVDW and CDW fluctuations, on the other hand, are peaked at the momentum $\mathbf{Q}_1 + \mathbf{Q}_2 = (\pi, \pi)$ and promote an *attractive* interpocket interaction $U < 0$ between the two electron pockets (see Fig. 4 and Appendix C). Solution of the linearized gap equation reveals that the leading eigenstate remains the s^{+-} one, but the eigenvalue is enhanced, $\Lambda = \sqrt{\Lambda_0^2 + \Lambda_U^2} + \Lambda_U$, with $\Lambda_U = \frac{N_e |U|}{2} > 0$. Therefore, fluctuations associated with these vestigial states may enhance the value of T_c promoted by spin-fluctuations pairing, without affecting the symmetry of the Cooper pair wave function. Similar conclusions have been found for the combination of pairing promoted by nematic fluctuations (peaked at $\mathbf{Q} = 0$) and magnetic fluctuations (peaked at \mathbf{Q}_1 and \mathbf{Q}_2) [23].

IV. CONCLUDING REMARKS

In summary, we showed that both biaxial tetragonal magnetic ground states of the pnictides—the nonuniform CSDW

and noncollinear SVC states—can melt in two-stage processes, giving rise to CDW and SVDW vestigial states, respectively. While both preserve the point-group and time-reversal symmetries, but break the translational symmetry of the iron square lattice, only the SVDW state also breaks inversion symmetry by entangling the spin-space handedness to a doubling of the real-space unit cell. Because in the iron superconductors the hybridization with the puckered As atoms already doubles the unit cell of the Fe square lattice, the CDW and SVDW states are more rigorously classified as intra-unit-cell orders. Recent experiments on $\text{Sr}_{1-x}\text{Na}_x\text{Fe}_2\text{As}_2$ [52] and $\text{Ba}_{1-x}\text{K}_x\text{Fe}_2\text{As}_2$ [53] found direct evidence for a low-temperature CSDW phase, which can support a CDW vestigial phase. It remains to be seen whether the tetragonal magnetic phase can be reached in these compounds without first crossing the stripe magnetic state. In contrast, in $\text{Ba}(\text{Fe}_{1-x}\text{Mn}_x)_2\text{As}_2$ [25], the tetragonal magnetic phase has been reported to exist over a wide doping range as the primary instability of the paramagnetic phase.

Beyond the physics of iron-based superconductors, our results establish the melting of double- \mathbf{Q} orders as a microscopic mechanism to create d -density wave states. The latter have been proposed to be realized in other strongly correlated systems, such as the pseudogap phase of underdoped cuprates [36] and the hidden-order phase of the heavy fermion compound URu_2Si_2 [37,54,55], mostly on a phenomenological basis. Whether our mechanism is directly applicable to those systems is an appealing topic for future investigation.

ACKNOWLEDGMENTS

We thank C. Batista, A. Boehmer, A. Chubukov, J. Kang, C. Meingast, R. Osborn, M. Schuett, and X. Wang for fruitful discussions. R.M.F. is supported by the U.S. Department of Energy, Office of Science, Basic Energy Sciences, under Award No. DE-SC0012336. S.A.K. is supported by the U.S. Department of Energy under Contract No. DE-AC02-76SF00515. E.B. was supported by the Israeli Science Foundation, by the US-Israel Binational Science Foundation, and by an Alon fellowship. We thank the hospitality of the Aspen Center for Physics, where this work was initiated. The Aspen Center for Physics is supported by National Science Foundation Grant No. PHY-1066293.

APPENDIX A: SADDLE-POINT EQUATIONS FOR THE SVDW ORDER

We start with the effective action for the magnetic order parameters:

$$S[\mathbf{M}_i] = \int_q \chi_q^{-1} (M_1^2 + M_2^2) + \frac{u}{2} \int_x (M_1^2 + M_2^2)^2 - \frac{g}{2} \int_x (M_1^2 - M_2^2)^2 + 2w \int_x (\mathbf{M}_1 \cdot \mathbf{M}_2)^2, \quad (\text{A1})$$

where $\int_q \equiv T \sum_{\omega_n} \int \frac{d^d q}{(2\pi)^d}$ and $\int_x \equiv \int_0^\beta d\tau \int d^d x$. To proceed, we use the identity

$$(\mathbf{M}_1 \cdot \mathbf{M}_2)^2 = \frac{1}{4}(M_1^2 + M_2^2)^2 - \frac{1}{4}(M_1^2 - M_2^2)^2 - (\mathbf{M}_1 \times \mathbf{M}_2)^2 \quad (\text{A2})$$

yielding

$$S[\mathbf{M}_i] = \int_q \chi_q^{-1} (M_1^2 + M_2^2) + \frac{(u+w)}{2} \int_x (M_1^2 + M_2^2)^2 - \frac{(g+w)}{2} \int_x (M_1^2 - M_2^2)^2 - 2w \int_x (\mathbf{M}_1 \times \mathbf{M}_2)^2. \quad (\text{A3})$$

Hereafter for simplicity we introduce the parameters $\tilde{g} = g + w$ and $\tilde{u} = u + w$. Since we are interested in the vestigial phase of the spin-vortex crystal, which has tetragonal symmetry, the nematic order parameter $\langle M_1^2 \rangle - \langle M_2^2 \rangle$ never condenses, and we can ignore the corresponding quartic term. Introducing the Hubbard-Stratonovich fields corresponding to the other two quadratic terms, we obtain

$$e^{-\frac{u}{2}(M_1^2 + M_2^2)^2} = \mathcal{N} \int d\psi e^{\frac{\psi^2}{2w} - \psi(M_1^2 + M_2^2)},$$

$$e^{2w(\mathbf{M}_1 \times \mathbf{M}_2) \cdot (\mathbf{M}_1 \times \mathbf{M}_2)} = \mathcal{N} \int d\boldsymbol{\varphi}_{\text{SVDW}} e^{\frac{\boldsymbol{\varphi}_{\text{SVDW}}^2}{2w} + 2\boldsymbol{\varphi}_{\text{SVDW}} \cdot (\mathbf{M}_1 \times \mathbf{M}_2)}. \quad (\text{A4})$$

Here, $\boldsymbol{\varphi}_{\text{SVDW}}$ is the SVDW vectorial order parameter whose mean value is given by $\langle \boldsymbol{\varphi}_{\text{SVDW}} \rangle = 2w \langle \mathbf{M}_1 \times \mathbf{M}_2 \rangle$. The field ψ is not an order parameter, and just renormalizes the magnetic correlation length via $\langle \psi \rangle = \tilde{u}(\langle M_1^2 \rangle + \langle M_2^2 \rangle)$, i.e., it corresponds to Gaussian magnetic fluctuations. Thus, the effective action is given by

$$S[\mathbf{M}_i, \psi, \boldsymbol{\varphi}_{\text{SVDW}}] = \int_q (\chi_q^{-1} + \psi)(M_1^2 + M_2^2) - 2 \int_x \boldsymbol{\varphi}_{\text{SVDW}} \cdot (\mathbf{M}_1 \times \mathbf{M}_2) + \frac{\boldsymbol{\varphi}_{\text{SVDW}}^2}{2w} - \frac{\psi^2}{2\tilde{u}}. \quad (\text{A5})$$

Approaching the SVDW phase from the paramagnetic state, we can integrate out the magnetic degrees of freedom, yielding an effective action for ψ and $\boldsymbol{\varphi}_{\text{SVDW}}$:

$$S_{\text{eff}}[\psi, \boldsymbol{\varphi}_{\text{SVDW}}] = \frac{\boldsymbol{\varphi}_{\text{SVDW}}^2}{2w} - \frac{\psi^2}{2\tilde{u}} + \frac{1}{2} \int_q \ln \left(\prod_i \lambda_{i,q} \right), \quad (\text{A6})$$

where $\lambda_{i,q}$ are the eigenvalues of the matrix A_{ij} corresponding to the Gaussian action in \mathbf{M}_i . The Gaussian part of the action can be rewritten in the convenient matrix form:

$$(\mathbf{M}_1 \ \mathbf{M}_2) \begin{pmatrix} \chi_q^{-1} + \psi & 0 & 0 & 0 & -\varphi_z & \varphi_y \\ 0 & \chi_q^{-1} + \psi & 0 & \varphi_z & 0 & -\varphi_x \\ 0 & 0 & \chi_q^{-1} + \psi & -\varphi_y & \varphi_x & 0 \\ 0 & \varphi_z & -\varphi_y & \chi_q^{-1} + \psi & 0 & 0 \\ -\varphi_z & 0 & \varphi_x & 0 & \chi_q^{-1} + \psi & 0 \\ \varphi_y & -\varphi_x & 0 & 0 & 0 & \chi_q^{-1} + \psi \end{pmatrix} \begin{pmatrix} \mathbf{M}_1 \\ \mathbf{M}_2 \end{pmatrix}. \quad (\text{A7})$$

Evaluation of the eigenvalues gives

$$S_{\text{eff}}[\psi, \boldsymbol{\varphi}_{\text{SVDW}}] = \frac{\boldsymbol{\varphi}_{\text{SVDW}}^2}{2w} - \frac{\psi^2}{2\tilde{u}} + \int_q \log [(\chi_q^{-1} + \psi)(\chi_q^{-1} + \psi + \boldsymbol{\varphi}_{\text{SVDW}})(\chi_q^{-1} + \psi - \boldsymbol{\varphi}_{\text{SVDW}})]. \quad (\text{A8})$$

So far our result is exact. To proceed, we employ the saddle-point approximation to determine the equations of state for ψ and $\boldsymbol{\varphi}_{\text{SVDW}}$, which corresponds to self-consistently accounting for the Gaussian magnetic fluctuations. The saddle-point equations become

$$\frac{\boldsymbol{\varphi}_{\text{SVDW}}}{w} = \int_q \frac{1}{\chi_q^{-1} + \psi - \boldsymbol{\varphi}_{\text{SVDW}}} - \int_q \frac{1}{\chi_q^{-1} + \psi + \boldsymbol{\varphi}_{\text{SVDW}}},$$

$$\frac{\psi}{\tilde{u}} = \int_q \frac{1}{\chi_q^{-1} + \psi - \boldsymbol{\varphi}_{\text{SVDW}}} + \int_q \frac{1}{\chi_q^{-1} + \psi + \boldsymbol{\varphi}_{\text{SVDW}}} + \int_q \frac{1}{\chi_q^{-1} + \psi}. \quad (\text{A9})$$

Since our focus is on the proximity to a finite-temperature magnetic transition, we ignore the spin dynamics and use the low-energy expansion for the spin susceptibility appropriate for anisotropic layered systems:

$$\chi_q^{-1} = r_0 + q_{\parallel}^2 + J_z \sin^2 \frac{q_z}{2}, \quad (\text{A10})$$

where $r_0 = a(T - T_N)$, $a > 0$, T_N is the mean-field magnetic transition temperature, $q_{\parallel}^2 = q_x^2 + q_y^2$, and J_z is the interlayer magnetic coupling. Defining the renormalized magnetic mass

$$r = r_0 + \psi \propto \xi^{-2}, \quad (\text{A11})$$

where ξ is the magnetic correlation length, we obtain

$$\begin{aligned} \varphi_{\text{SVDW}} &= w \left[\int_q \frac{1}{r + q_{\parallel}^2 + J_z \sin^2 \frac{q_z}{2} - \varphi_{\text{SVDW}}} - \int_q \frac{1}{r + q_{\parallel}^2 + J_z \sin^2 \frac{q_z}{2} + \varphi_{\text{SVDW}}} \right], \\ r &= r_0 + \tilde{u} \left[\int_q \frac{1}{r + q_{\parallel}^2 + J_z \sin^2 \frac{q_z}{2} - \varphi_{\text{SVDW}}} + \int_q \frac{1}{r + q_{\parallel}^2 + J_z \sin^2 \frac{q_z}{2} + \varphi_{\text{SVDW}}} + \int_q \frac{1}{r + q_{\parallel}^2 + J_z \sin^2 \frac{q_z}{2}} \right]. \end{aligned} \quad (\text{A12})$$

The integrals can be evaluated in a straightforward way (we consider only the $\omega_n = 0$ contribution to the sum over Matsubara frequencies, since we are interested in the finite temperature transition):

$$\begin{aligned} \int_q \frac{1}{q_{\parallel}^2 + J_z \sin^2 \frac{q_z}{2} + a} &= \frac{T_N}{4\pi} \int_0^{2\pi} \frac{dq_z}{2\pi} \int_{J_z \sin^2 \frac{q_z}{2} + a}^{\Lambda^2} \frac{dx}{x} \\ &= \frac{T_N}{4\pi} \int_0^{2\pi} \frac{dq_z}{2\pi} \ln \left(\frac{\Lambda^2}{J_z \sin^2 \frac{q_z}{2} + a} \right) \\ &= \frac{T_N}{2\pi} [\ln 2\Lambda - \ln(\sqrt{J_z + a} + \sqrt{a})]. \end{aligned} \quad (\text{A13})$$

Defining the renormalized critical temperature $\tilde{r}_0 = a(T - \tilde{T}_N)$ via

$$\tilde{r}_0 = r_0 + \frac{3\tilde{u}T_N}{2\pi} \ln \frac{2\Lambda}{\sqrt{J_z}}, \quad (\text{A14})$$

we obtain the self-consistent equations

$$\begin{aligned} \varphi_{\text{SVDW}} &= \frac{wT_N}{2\pi} \ln \frac{\sqrt{J_z + r + \varphi_{\text{SVDW}}} + \sqrt{r + \varphi_{\text{SVDW}}}}{\sqrt{J_z + r - \varphi_{\text{SVDW}}} + \sqrt{r - \varphi_{\text{SVDW}}}}, \\ r &= \tilde{r}_0 - \frac{\tilde{u}T_N}{2\pi} \ln \left[\frac{(\sqrt{J_z + r + \varphi_{\text{SVDW}}} + \sqrt{r + \varphi_{\text{SVDW}}})(\sqrt{J_z + r - \varphi_{\text{SVDW}}} + \sqrt{r - \varphi_{\text{SVDW}}})(\sqrt{J_z + r} + \sqrt{r})}{J_z^{3/2}} \right]. \end{aligned} \quad (\text{A15})$$

For simplicity, we define the renormalized parameters $(\tilde{w}, \tilde{u}) \equiv (w, u) \frac{T_N}{2\pi}$ as well as $\alpha \equiv \frac{\tilde{u}}{\tilde{w}} = \frac{u}{w} + 1$ and $\tilde{J}_z \equiv J_z / \tilde{w}$. Then the equations can be written as

$$\begin{aligned} \varphi_{\text{SVDW}} &= \ln \frac{\sqrt{\tilde{J}_z + r + \varphi_{\text{SVDW}}} + \sqrt{r + \varphi_{\text{SVDW}}}}{\sqrt{\tilde{J}_z + r - \varphi_{\text{SVDW}}} + \sqrt{r - \varphi_{\text{SVDW}}}}, \\ r &= \tilde{r}_0 - \alpha \ln \left[\frac{(\sqrt{\tilde{J}_z + r + \varphi_{\text{SVDW}}} + \sqrt{r + \varphi_{\text{SVDW}}})(\sqrt{\tilde{J}_z + r - \varphi_{\text{SVDW}}} + \sqrt{r - \varphi_{\text{SVDW}}})(\sqrt{\tilde{J}_z + r} + \sqrt{r})}{\tilde{J}_z^{3/2}} \right], \end{aligned} \quad (\text{A16})$$

where r , \tilde{r}_0 , and φ_{SVDW} were rescaled by \tilde{w} as well. The SVDW transition temperature can be obtained by linearizing the equations around $\varphi_{\text{SVDW}} = 0$. From the first equation, we obtain the correlation length r_1 at the SVDW transition:

$$r_1 = \frac{\sqrt{\tilde{J}_z^2 + 4} - \tilde{J}_z}{2}, \quad (\text{A17})$$

which, when substituted in the second equation, gives the SVDW transition temperature $\tilde{r}_{0,\text{SVDW}}$

$$\tilde{r}_{0,\text{SVDW}} = \frac{\sqrt{\tilde{J}_z^2 + 4} - \tilde{J}_z}{2} + 3\alpha \ln \left(\frac{\sqrt{\sqrt{\tilde{J}_z^2 + 4} + \tilde{J}_z} + \sqrt{\sqrt{\tilde{J}_z^2 + 4} - \tilde{J}_z}}{\sqrt{2\tilde{J}_z}} \right). \quad (\text{A18})$$

The magnetic transition temperature $\tilde{r}_{0,\text{mag}}$ is signaled by the vanishing of the renormalized magnetic mass, i.e., the lowest eigenvalue of the Eq. (A7), $r - \varphi_{\text{SVDW}}$. Therefore, it takes place when r reaches the value r_2 determined implicitly by

$$r_2 = \ln \frac{\sqrt{\tilde{J}_z + 2r_2} + \sqrt{2r_2}}{\sqrt{\tilde{J}_z}}. \quad (\text{A19})$$

The magnetic transition temperature is therefore given by

$$\tilde{r}_{0,\text{mag}} = r_2(1 + \alpha) + \alpha \ln \left[\frac{\sqrt{\tilde{J}_z + r_2} + \sqrt{r_2}}{\sqrt{\tilde{J}_z}} \right]. \quad (\text{A20})$$

The SVDW and magnetic transitions are split when $\tilde{r}_{0,\text{SVDW}} > \tilde{r}_{0,\text{mag}}$. The region in the $(\frac{u}{w}, \tilde{J}_z)$ parameter space where this condition is satisfied corresponds to the shaded area of Fig. 3 in the main text (recall that $\frac{u}{w} = \alpha - 1$).

To determine the character of the SVDW transition, we can expand \tilde{r}_0 for small φ_{SVDW} . Substituting $r = r_1 + a\varphi_{\text{SVDW}}^2$ in the first equation of (A16) and expanding for small φ_{SVDW} gives the coefficient of the quadratic term:

$$a = \frac{8 + 3\tilde{J}_z^2}{12\sqrt{\tilde{J}_z^2 + 4}}. \quad (\text{A21})$$

Substituting it in the second equation of (A16) and collecting the quadratic terms in φ_{SVDW} yields

$$\tilde{r}_0(\varphi_{\text{SVDW}}) \approx \tilde{r}_{0,\text{SVDW}} + \left[\frac{16 + 3\tilde{J}_z^2(2 + \alpha)}{24\sqrt{\tilde{J}_z^2 + 4}} \right] \varphi_{\text{SVDW}}^2. \quad (\text{A22})$$

Therefore, because the coefficient is always positive, the solution with $\varphi_{\text{SVDW}} \neq 0$ is achieved at a larger temperature than the solution with $\varphi_{\text{SVDW}} = 0$; in other words, $\tilde{r}_0(\varphi_{\text{SVDW}} > 0) > \tilde{r}_0(\varphi_{\text{SVDW}} \rightarrow 0)$. As a result, the SVDW transition is first order within the saddle-point approximation, even when it is split from the magnetic transition.

APPENDIX B: DERIVATION OF THE GINZBURG-LANDAU FREE ENERGY

Our starting point is a three-band model with a circular hole pocket h centered at $(0,0)$ and two elliptical electron pockets $e_{1,2}$ centered at $\mathbf{Q}_1 = (\pi, 0)$ and $\mathbf{Q}_2 = (0, \pi)$, respectively. The band dispersions can be conveniently parametrized by [8]

$$\begin{aligned} \xi_{h,\mathbf{k}} &= -\xi_{\mathbf{k}} = -\frac{k^2}{2m} + \varepsilon_0, \\ \xi_{e_1,\mathbf{k}+\mathbf{Q}_1} &= \xi_{\mathbf{k}} - (\delta_0 + \delta_2 \cos 2\theta), \\ \xi_{e_2,\mathbf{k}+\mathbf{Q}_2} &= \xi_{\mathbf{k}} - (\delta_0 - \delta_2 \cos 2\theta). \end{aligned} \quad (\text{B1})$$

Here, δ_0 is proportional to the chemical potential and δ_2 to the ellipticity of the electron pockets. The angle θ is measured relative to the k_x axis. The noninteracting Hamiltonian is therefore given by (hereafter sums over repeated spin indices are implicitly assumed):

$$H_0 = \sum_{\mathbf{k}} \xi_{h,\mathbf{k}} c_{h,\mathbf{k}\sigma}^\dagger c_{h,\mathbf{k}\sigma} + \sum_{\mathbf{k}} \xi_{e_1,\mathbf{k}} c_{e_1,\mathbf{k}\sigma}^\dagger c_{e_1,\mathbf{k}\sigma} + \sum_{\mathbf{k}} \xi_{e_2,\mathbf{k}} c_{e_2,\mathbf{k}\sigma}^\dagger c_{e_2,\mathbf{k}\sigma}. \quad (\text{B2})$$

These electronic states couple to the magnetic order parameters \mathbf{M}_1 and \mathbf{M}_2 according to

$$H_{\text{mag}} = \sum_{\mathbf{k},i} \mathbf{M}_i \cdot (c_{e_i,\mathbf{k}\alpha}^\dagger \boldsymbol{\sigma}_{\alpha\beta} c_{h,\mathbf{k}\beta} + \text{H.c.}). \quad (\text{B3})$$

In principle, this last term can be obtained via a Hubbard-Stratonovich transformation of the original interaction terms projected into the magnetic channel, as shown in Ref. [8]. Here, because we are interested in the higher-order couplings of the action involving the \mathbf{M}_i order parameters, we neglect these interaction terms, since they only affect the quadratic terms of the action.

1. Absence of magnetic field

In the case where there is no external magnetic field, we focus on the two types of fermionic order that couple directly to the SVDW order parameter, $\mathbf{M}_1 \times \mathbf{M}_2$, and to the CDW order parameter $\mathbf{M}_1 \cdot \mathbf{M}_2$. Thus, we introduce the $\mathbf{Q}_1 + \mathbf{Q}_2 = (\pi, \pi)$ spin-current density wave Δ'_S (i.e., a purely imaginary SDW) and the checkerboard charge order Δ'_C (i.e., a purely real CDW) defined by

$$\mathcal{H}_{iS} = i \sum_{\mathbf{k}} \Delta'_S \cdot \boldsymbol{\sigma}_{\alpha\beta} (c_{e_2,\mathbf{k}\alpha}^\dagger c_{e_1,\mathbf{k}\beta} - c_{e_1,\mathbf{k}\alpha}^\dagger c_{e_2,\mathbf{k}\beta}), \quad \mathcal{H}_C = \sum_{\mathbf{k}} \Delta'_C \delta_{\alpha\beta} (c_{e_2,\mathbf{k}\alpha}^\dagger c_{e_1,\mathbf{k}\beta} + c_{e_1,\mathbf{k}\alpha}^\dagger c_{e_2,\mathbf{k}\beta}). \quad (\text{B4})$$

To proceed, we introduce the six-dimensional Nambu operator

$$\Psi_{\mathbf{k}}^\dagger = (c_{h,\mathbf{k}\uparrow}^\dagger \quad c_{h,\mathbf{k}\downarrow}^\dagger \quad c_{e_1,\mathbf{k}\uparrow}^\dagger \quad c_{e_1,\mathbf{k}\downarrow}^\dagger \quad c_{e_2,\mathbf{k}\uparrow}^\dagger \quad c_{e_2,\mathbf{k}\downarrow}^\dagger), \quad (\text{B5})$$

which allows us to write the fermionic action in the compact form:

$$S = - \int_k \Psi_k^\dagger \hat{\mathcal{G}}_k^{-1} \Psi_k + S_0[M_i^2]. \quad (\text{B6})$$

In the previous expression, $S_0[M_i^2]$ corresponds to the terms M_i^2 that arise from the decoupling of the fermionic interactions. As we explained above, these terms can be ignored for our purposes. The total Green's function is given by

$$\hat{G}_k^{-1} = (\hat{G}_k^{(0)})^{-1} - \hat{V}_{\text{mag}} - \hat{V}_{iS} - \hat{V}_C. \quad (\text{B7})$$

The bare part is

$$\hat{G}_k^{(0)} = \begin{pmatrix} G_{h,k} & 0 & 0 & 0 & 0 & 0 \\ 0 & G_{h,k} & 0 & 0 & 0 & 0 \\ 0 & 0 & G_{e_1,k} & 0 & 0 & 0 \\ 0 & 0 & 0 & G_{e_1,k} & 0 & 0 \\ 0 & 0 & 0 & 0 & G_{e_2,k} & 0 \\ 0 & 0 & 0 & 0 & 0 & G_{e_2,k} \end{pmatrix}, \quad (\text{B8})$$

where $G_{i,k}^{-1} = i\omega_n - \xi_{i,\mathbf{k}}$ are noninteracting single-particle Green's functions. The interacting parts are

$$\hat{V}_{\text{mag}} = \begin{pmatrix} 0 & 0 & -M_{1,z} & -M_{1,x} + iM_{1,y} & -M_{2,z} & -M_{2,x} + iM_{2,y} \\ 0 & 0 & -M_{1,x} - iM_{1,y} & M_{1,z} & -M_{2,x} - iM_{2,y} & M_{2,z} \\ -M_{1,z} & -M_{1,x} + iM_{1,y} & 0 & 0 & 0 & 0 \\ -M_{1,x} - iM_{1,y} & M_{1,z} & 0 & 0 & 0 & 0 \\ -M_{2,z} & -M_{2,x} + iM_{2,y} & 0 & 0 & 0 & 0 \\ -M_{2,x} - iM_{2,y} & M_{2,z} & 0 & 0 & 0 & 0 \end{pmatrix} \quad (\text{B9})$$

and

$$\hat{V}_{iS} = \begin{pmatrix} 0 & 0 & 0 & 0 & 0 & 0 \\ 0 & 0 & 0 & 0 & 0 & 0 \\ 0 & 0 & 0 & 0 & i\Delta''_{S,z} & i(\Delta''_{S,x} - i\Delta''_{S,y}) \\ 0 & 0 & 0 & 0 & i(\Delta''_{S,x} + i\Delta''_{S,y}) & -i\Delta''_{S,z} \\ 0 & 0 & -i\Delta''_{S,z} & -i(\Delta''_{S,x} - i\Delta''_{S,y}) & 0 & 0 \\ 0 & 0 & -i(\Delta''_{S,x} + i\Delta''_{S,y}) & i\Delta''_{S,z} & 0 & 0 \end{pmatrix} \quad (\text{B10})$$

as well as

$$\hat{V}_C = \begin{pmatrix} 0 & 0 & 0 & 0 & 0 & 0 \\ 0 & 0 & 0 & 0 & 0 & 0 \\ 0 & 0 & 0 & 0 & -\Delta'_C & 0 \\ 0 & 0 & 0 & 0 & 0 & -\Delta'_C \\ 0 & 0 & -\Delta'_C & 0 & 0 & 0 \\ 0 & 0 & 0 & -\Delta'_C & 0 & 0 \end{pmatrix}. \quad (\text{B11})$$

It is now straightforward to integrate out the fermions and obtain the effective magnetic action

$$S_{\text{eff}}[\mathbf{M}_1, \mathbf{M}_2, \Delta''_S, \Delta'_C] = -\text{Tr} \ln[1 - \hat{G}_0(\hat{V}_{\text{mag}} + \hat{V}_{iS} + \hat{V}_C)] \approx \sum_n \frac{1}{n} \text{Tr}[\hat{G}_0(\hat{V}_{\text{mag}} + \hat{V}_{iS} + \hat{V}_C)]^n, \quad (\text{B12})$$

where, in the last step, we expanded for small M_1, M_2 . Here, $\text{Tr}(\dots)$ refers to the sum over momentum, frequency, and Nambu indices. A straightforward evaluation gives, to the leading order in the coupling between Δ''_S, Δ'_C , and \mathbf{M}_i :

$$S_{\text{eff}}[\mathbf{M}_1, \mathbf{M}_2, \Delta''_S, \Delta'_C] = S[\mathbf{M}_1, \mathbf{M}_2] + \lambda \Delta''_S \cdot (\mathbf{M}_1 \times \mathbf{M}_2) - \lambda \Delta'_C (\mathbf{M}_1 \cdot \mathbf{M}_2), \quad (\text{B13})$$

with the coefficient

$$\lambda = 4 \int_k G_{h,k} G_{e_1,k} G_{e_2,k}. \quad (\text{B14})$$

For perfect nesting, $\delta_0 = \delta_2 = 0$, this coefficient vanishes. For a system in proximity to a finite temperature phase transition, expansion in powers of δ_0 gives

$$\begin{aligned} \lambda &\approx 4\rho_F T \sum_n \int d\xi \frac{1}{(i\omega_n + \xi)(i\omega_n - \xi + \delta_0)^2}, \\ \lambda &\approx -8\delta_0 \rho_F T \sum_n \int d\xi \frac{1}{(i\omega_n + \xi)(i\omega_n - \xi)^3}, \\ \lambda &\approx -\left(\frac{\delta_0}{T}\right) \frac{7\zeta(3)\rho_F}{2\pi^2 T}, \end{aligned} \quad (\text{B15})$$

where ρ_F is the density of states at the Fermi level. Therefore, it is clear that a spin-current density-wave Δ'_S parallel to φ_{SVDW} is triggered by the SVDW order parameter $\varphi_{\text{SVDW}} \propto \mathbf{M}_1 \times \mathbf{M}_2$, whereas a checkerboard charge order Δ'_C is triggered by the CDW order parameter $\varphi_{\text{CDW}} \propto \mathbf{M}_1 \cdot \mathbf{M}_2$.

2. Nonzero magnetic field

In the presence of a magnetic field, additional types of fermionic order are triggered by the condensation of the SVDW and CDW order parameters. To show that, we first introduce the Zeeman coupling between the uniform field \mathbf{H} and the electrons:

$$H_{\text{Zeeman}} = \sum_{\mathbf{k}, i} \mathbf{H} \cdot \boldsymbol{\sigma}_{\alpha\beta} c_{i, \mathbf{k}\alpha}^\dagger c_{i, \mathbf{k}\beta}. \quad (\text{B16})$$

We also introduce the $\mathbf{Q}_1 + \mathbf{Q}_2 = (\pi, \pi)$ charge-current density-wave Δ''_C (i.e., a purely imaginary CDW) and the spin density-wave Δ'_S (i.e., a purely real SDW) defined by

$$\mathcal{H}_S = \sum_{\mathbf{k}} \Delta'_S \cdot \boldsymbol{\sigma}_{\alpha\beta} (c_{e_2, \mathbf{k}\alpha}^\dagger c_{e_1, \mathbf{k}\beta} + c_{e_1, \mathbf{k}\alpha}^\dagger c_{e_2, \mathbf{k}\beta}), \quad \mathcal{H}_{iC} = i \sum_{\mathbf{k}} \Delta''_C \delta_{\alpha\beta} (c_{e_2, \mathbf{k}\alpha}^\dagger c_{e_1, \mathbf{k}\beta} - c_{e_1, \mathbf{k}\alpha}^\dagger c_{e_2, \mathbf{k}\beta}). \quad (\text{B17})$$

Following the same steps as in the previous subsection, we obtain the expanded action

$$\mathcal{S}_{\text{eff}}[\mathbf{M}_1, \mathbf{M}_2, \Delta'_S, \Delta''_C] \approx \sum_n \frac{1}{n} \text{Tr}[\hat{\mathcal{G}}_0(\hat{V}_{\text{mag}} + \hat{V}_S + \hat{V}_{iC} + \hat{V}_{\text{Zeeman}})]^n, \quad (\text{B18})$$

where the Nambu-space matrices are given by

$$\hat{V}_{\text{Zeeman}} = \begin{pmatrix} -H_z & -H_x + iH_y & 0 & 0 & 0 & 0 \\ -H_x - iH_y & H_z & 0 & 0 & 0 & 0 \\ 0 & 0 & -H_z & -H_x + iH_y & 0 & 0 \\ 0 & 0 & -H_x - iH_y & h_z & 0 & 0 \\ 0 & 0 & 0 & 0 & -H_z & -H_x + iH_y \\ 0 & 0 & 0 & 0 & -H_x - iH_y & H_z \end{pmatrix} \quad (\text{B19})$$

and

$$\hat{V}_{iC} = \begin{pmatrix} 0 & 0 & 0 & 0 & 0 & 0 \\ 0 & 0 & 0 & 0 & 0 & 0 \\ 0 & 0 & 0 & 0 & i\Delta''_C & 0 \\ 0 & 0 & 0 & 0 & 0 & i\Delta''_C \\ 0 & 0 & -i\Delta''_C & 0 & 0 & 0 \\ 0 & 0 & 0 & -i\Delta''_C & 0 & 0 \end{pmatrix} \quad (\text{B20})$$

as well as

$$\hat{V}_S = \begin{pmatrix} 0 & 0 & 0 & 0 & 0 & 0 \\ 0 & 0 & 0 & 0 & 0 & 0 \\ 0 & 0 & 0 & 0 & -\Delta'_{S,z} & -(\Delta'_{S,x} - i\Delta'_{S,y}) \\ 0 & 0 & 0 & 0 & -(\Delta'_{S,x} + i\Delta'_{S,y}) & \Delta'_{S,z} \\ 0 & 0 & -\Delta'_{S,z} & -(\Delta'_{S,x} - i\Delta'_{S,y}) & 0 & 0 \\ 0 & 0 & -(\Delta'_{S,x} + i\Delta'_{S,y}) & \Delta'_{S,z} & 0 & 0 \end{pmatrix}. \quad (\text{B21})$$

A straightforward evaluation yields, to leading order in the magnetic field

$$\begin{aligned} \mathcal{S}_{\text{eff}} &= \mathcal{S}_{\text{eff}}[\mathbf{H} = 0] + \zeta[(\mathbf{H} \cdot \mathbf{M}_1)^2 + (\mathbf{H} \cdot \mathbf{M}_2)^2] + \gamma[\Delta''_C \mathbf{H} \cdot (\mathbf{M}_1 \times \mathbf{M}_2) + (\mathbf{H} \cdot \Delta'_S)(\mathbf{M}_1 \cdot \mathbf{M}_2)] \\ &+ \eta[(\mathbf{M}_1 \cdot \mathbf{H})(\mathbf{M}_2 \cdot \Delta'_S) + (\mathbf{M}_2 \cdot \mathbf{H})(\mathbf{M}_1 \cdot \Delta'_S)], \end{aligned} \quad (\text{B22})$$

where we neglected all isotropic biquadratic terms of the form $H^2 M_i^2$. The coefficients are given by

$$\begin{aligned} \zeta &= 4 \int_{\mathbf{k}} G_{h,k}^2 G_{e_1,k}^2, \\ \gamma &= 4 \int_{\mathbf{k}} G_{h,k} G_{e_1,k} G_{e_2,k} (G_{e_1,k} + G_{e_2,k} - G_{h,k}), \\ \eta &= 4 \int_{\mathbf{k}} G_{h,k}^2 G_{e_1,k} G_{e_2,k}. \end{aligned} \quad (\text{B23})$$

It is useful to perform an expansion around perfect nesting, $\delta_0 = \delta_2 = 0$. The coefficients ζ and η become identical in this limit:

$$\zeta = \eta = \frac{\rho_F}{T^2} \left(\frac{7\zeta(3)}{2\pi^2} \right). \quad (\text{B24})$$

The fact that $\zeta > 0$ implies that the magnetic field induces an easy plane, rather than an easy axis anisotropy. As for the coefficient η , it remains zero in all orders in perturbation theory if an infinite bandwidth is assumed. However, keeping the top of the hole pocket W (or bottom of the electron pocket) throughout the calculation gives

$$\gamma \approx \frac{\rho_F}{T^2} \left(\frac{W}{T} \right)^{-2}. \quad (\text{B25})$$

The fact that $\gamma \neq 0$ implies that, in the presence of a uniform field, the SVDW order parameter $\varphi_{\text{SVDW}} \propto \mathbf{M}_1 \times \mathbf{M}_2$ also triggers a charge-current density-wave Δ''_C , whereas the CDW order parameter $\varphi_{\text{CDW}} \propto \mathbf{M}_1 \cdot \mathbf{M}_2$ triggers a spin density wave of same period, Δ'_S . Although this was expected by symmetry, here we have microscopic expressions for the corresponding Ginzburg-Landau coefficients. It is interesting then to compare the coefficient γ in Eq. (B22), which determines the amplitudes of Δ''_C and Δ'_S , to the coefficient λ in Eq. (B13), which determines the amplitudes of Δ''_S and Δ'_C . We find that

$$\frac{\gamma H}{\lambda} \approx -2.3 \left(\frac{T^2 H}{W^2 \delta_0} \right). \quad (\text{B26})$$

Therefore, for pnictides whose band dispersions do not deviate strongly from perfect nesting, and whose bandwidths are not too large either, it is conceivable that the two coupling constants γH and λ will be of similar order for moderate values of the magnetic field H . As a result, the charge-current density wave and the spin density wave generated in the presence of the field could be as large as the spin-current density wave and the charge density wave generated in the absence of the field.

APPENDIX C: SUPERCONDUCTING PAIRING INTERACTIONS

Here we show explicitly that fluctuations associated with an imaginary SDW instability or with a real CDW instability give rise to attractive pairing interactions. For our purposes, it is sufficient to consider only the two Fermi pockets connected by the momentum transfer $\mathbf{Q} = (\pi, \pi)$ associated with these two ordered states. To simplify the notation, here we will denote the fermionic operators associated with these bands by $d_{\mathbf{k}\sigma}$ and $f_{\mathbf{k}\sigma}$. In both cases, \mathbf{k} is measured relative to the center of each Fermi pocket. Consider first the action describing the coupling between the electrons and the complex SDW bosonic field $\Delta_S = \Delta_S \hat{\mathbf{z}}$ (for simplicity, we consider it polarized along the z axis):

$$S = - \int_k [(i\omega_n - \varepsilon_{d,\mathbf{k}}) d_{\mathbf{k}\sigma}^\dagger d_{\mathbf{k}\sigma} + (i\omega_n - \varepsilon_{f,\mathbf{k}}) f_{\mathbf{k}\sigma}^\dagger f_{\mathbf{k}\sigma}] + g \int_{k,q} \sigma (\Delta'_{S,-k-q} d_{\mathbf{k}\sigma}^\dagger f_{\mathbf{q}\sigma} + \Delta'_{S,-k-q} f_{\mathbf{k}\sigma}^\dagger d_{\mathbf{q}\sigma}) + g \int_{k,q} \sigma (i \Delta''_{S,-k-q} d_{\mathbf{k}\sigma}^\dagger f_{\mathbf{q}\sigma} - i \Delta''_{S,-k-q} f_{\mathbf{k}\sigma}^\dagger d_{\mathbf{q}\sigma}) + \int_k \chi_S^{-1}(\mathbf{k}, \Omega_n) \Delta'_{S,k} \Delta'_{S,-k} + \int_k \chi_{iS}^{-1}(\mathbf{k}, \Omega_n) \Delta''_{S,k} \Delta''_{S,-k}, \quad (\text{C1})$$

where $k \equiv (\mathbf{k}, \omega_n)$, $f_k \equiv T \sum_n \int \frac{d^d k}{(2\pi)^d}$ (with the appropriate bosonic Ω_n or fermionic ω_n Matsubara frequency), and we left implicit the sum over spin indices, as well as the dependence of the fermionic operators on the fermionic Matsubara frequencies. χ_S and χ_{iS} are the susceptibilities associated with the real and imaginary SDW, and g is the coupling constant. Note that, because \mathbf{Q} is a commensurate vector, the real and imaginary SDW fields are independent. Introducing the four-dimensional Nambu operator

$$\Psi_{\mathbf{k}}^\dagger = (d_{\mathbf{k}\uparrow}^\dagger \quad d_{-\mathbf{k}\downarrow} \quad f_{\mathbf{k}\uparrow}^\dagger \quad f_{-\mathbf{k}\downarrow}), \quad (\text{C2})$$

the action can be written conveniently as

$$S = - \int_k \Psi_{\mathbf{k}}^\dagger (i\omega_n \hat{1} - \hat{\varepsilon}_{\mathbf{k}}) \Psi_{\mathbf{k}} + \int_k \chi_S^{-1}(\mathbf{k}, \Omega_n) \Delta'_{S,k} \Delta'_{S,-k} + \int_k \chi_{iS}^{-1}(\mathbf{k}, \Omega_n) \Delta''_{S,k} \Delta''_{S,-k} + g \int_{k,q} \Delta'_{S,-k-q} \Psi_{\mathbf{k}}^\dagger \hat{\rho}_S \Psi_{\mathbf{q}} + g \int_{k,q} \Delta''_{S,-k-q} \Psi_{\mathbf{k}}^\dagger \hat{\rho}_{iS} \Psi_{\mathbf{q}}, \quad (\text{C3})$$

where we defined the 4×4 matrices

$$\hat{\varepsilon}_{\mathbf{k}} = \begin{pmatrix} \varepsilon_{d,\mathbf{k}} \tau_z & 0 \\ 0 & \varepsilon_{f,\mathbf{k}} \tau_z \end{pmatrix}, \quad \hat{\rho}_S = \begin{pmatrix} 0 & \tau_0 \\ \tau_0 & 0 \end{pmatrix} \equiv \tau_0 \otimes \sigma_x, \quad \hat{\rho}_{iS} = \begin{pmatrix} 0 & i\tau_z \\ -i\tau_z & 0 \end{pmatrix} \equiv -\tau_z \otimes \sigma_y, \quad (\text{C4})$$

where τ_i are the Pauli matrices and 0 denotes the 2×2 matrix whose elements are all zero. To obtain the Eliashberg-like gap equations, we need to solve Dyson's equation

$$\hat{G}_k^{-1} = \hat{G}_{0,k}^{-1} - \hat{\Sigma}_k, \quad (\text{C5})$$

with $\hat{G}_{0,k}^{-1} = i\omega_n \hat{1} - \hat{\varepsilon}_{\mathbf{k}}$ and the one-loop self-energy

$$\hat{\Sigma}_k = g^2 \int_q \chi_S(k-q) \hat{\rho}_S \hat{G}_q \hat{\rho}_S + g^2 \int_q \chi_{iS}(k-q) \hat{\rho}_{iS} \hat{G}_q \hat{\rho}_{iS}. \quad (\text{C6})$$

It is convenient to parametrize the self-energy by

$$\hat{\Sigma}_k = (\hat{1} - \hat{Z}_k) i\omega_n + \hat{W}_k + \hat{\xi}_k, \quad (\text{C7})$$

where we introduced the imaginary normal components $Z_{\mu,k}$, the real normal components $\xi_{\mu,k}$, and the anomalous components $W_{\mu,k}$ ($\mu = d, f$ is a band index):

$$\hat{Z}_k = \begin{pmatrix} Z_{d,k} \tau_0 & 0 \\ 0 & Z_{f,k} \tau_0 \end{pmatrix}, \quad \hat{W}_k = \begin{pmatrix} W_{d,k} \tau_x & 0 \\ 0 & W_{f,k} \tau_x \end{pmatrix}, \quad \hat{\xi}_k = \begin{pmatrix} \xi_{d,k} \tau_z & 0 \\ 0 & \xi_{f,k} \tau_z \end{pmatrix}. \quad (\text{C8})$$

The superconducting gap in band μ is therefore proportional to $W_{\mu,k}$. Using Eqs. (C5) and (C7), it is straightforward to invert the matrix and obtain \hat{G} . Substituting it in (C6) and comparing back with Eq. (C7), we arrive at a set of six self-consistent equations. Four of them have the same form for either real or imaginary SDW, namely, the two equations that renormalize the dispersion $\tilde{\varepsilon}_{a,k} = \xi_{a,k} + \varepsilon_{\mathbf{k}}$ and the two that renormalize the quasiparticle weights $Z_{\mu,\mathbf{k}}$. However, the two self-consistent gap equations acquire different forms:

$$\begin{aligned} W_{d,k} &= - \int_q [g^2 \chi_S(k-q)] \frac{W_{f,q}}{D_{f,q}} - \int_q [-g^2 \chi_{iS}(k-q)] \frac{W_{f,q}}{D_{f,q}}, \\ W_{f,k} &= - \int_q [g^2 \chi_S(k-q)] \frac{W_{d,q}}{D_{d,q}} - \int_q [-g^2 \chi_{iS}(k-q)] \frac{W_{d,q}}{D_{d,q}}, \end{aligned} \quad (\text{C9})$$

where we defined $D_{\mu,q}^2 = Z_{\mu,q}^2 \omega_n^2 + \tilde{\varepsilon}_{\mu,q}^2 + W_{\mu,q}^2$. From the form of these equations, it becomes clear that while the fluctuations near the real SDW instability give rise to a repulsive interband pairing interaction $V_{df} \propto g^2 \chi_S$, the fluctuations near the imaginary SDW instability promote an attractive interband pairing interaction $V_{df} \propto -g^2 \chi_{iS}$. This difference relies ultimately on the different structures of the matrix elements (C4) in Nambu space.

A similar analysis can be performed in the charge channel:

$$\begin{aligned} S &= - \int_k [(i\omega_n - \varepsilon_{d,\mathbf{k}}) d_{\mathbf{k}\sigma}^\dagger d_{\mathbf{k}\sigma} + (i\omega_n - \varepsilon_{f,\mathbf{k}}) f_{\mathbf{k}\sigma}^\dagger f_{\mathbf{k}\sigma}] + g \int_{k,q} (\Delta'_{C,-k-q} d_{\mathbf{k}\sigma}^\dagger f_{\mathbf{q}\sigma} + \Delta'_{C,-k-q} f_{\mathbf{k}\sigma}^\dagger d_{\mathbf{q}\sigma}) \\ &+ g \int_{k,q} (i \Delta''_{C,-k-q} d_{\mathbf{k}\sigma}^\dagger f_{\mathbf{q}\sigma} - i \Delta''_{C,-k-q} f_{\mathbf{k}\sigma}^\dagger d_{\mathbf{q}\sigma}) + \int_k \chi_C^{-1}(\mathbf{k}, \Omega_n) \Delta'_{C,k} \Delta'_{C,-k} + \int_k \chi_{iC}^{-1}(\mathbf{k}, \Omega_n) \Delta''_{C,k} \Delta''_{C,-k}. \end{aligned} \quad (\text{C10})$$

In Nambu space, we obtain

$$\begin{aligned} S &= - \int_k \Psi_{\mathbf{k}}^\dagger (i\omega_n \hat{1} - \hat{\varepsilon}_{\mathbf{k}}) \Psi_{\mathbf{k}} + \int_k \chi_C^{-1}(\mathbf{k}, \Omega_n) \Delta'_{C,k} \Delta'_{C,-k} + \int_k \chi_{iC}^{-1}(\mathbf{k}, \Omega_n) \Delta''_{C,k} \Delta''_{C,-k} \\ &+ g \int_{k,q} \Delta'_{C,-k-q} \Psi_{\mathbf{k}}^\dagger \hat{\rho}_C \Psi_{\mathbf{p}} + g \int_{k,q} \Delta''_{C,-k-q} \Psi_{\mathbf{k}}^\dagger \hat{\rho}_{iC} \Psi_{\mathbf{p}}, \end{aligned} \quad (\text{C11})$$

where we defined the 4×4 matrices

$$\hat{\rho}_C = \begin{pmatrix} 0 & \tau_z \\ \tau_z & 0 \end{pmatrix} \equiv \tau_z \otimes \sigma_x, \quad \hat{\rho}_{iC} = \begin{pmatrix} 0 & i\tau_0 \\ -i\tau_0 & 0 \end{pmatrix} \equiv -\tau_0 \otimes \sigma_y. \quad (\text{C12})$$

Solving the one-loop Dyson equation, we obtain the two self-consistent gap equations

$$\begin{aligned} W_{d,k} &= - \int_q [-g^2 \chi_C(k-q)] \frac{W_{f,q}}{D_{f,q}} - \int_q [g^2 \chi_{iC}(k-q)] \frac{W_{f,q}}{D_{f,q}}, \\ W_{f,k} &= - \int_q [-g^2 \chi_C(k-q)] \frac{W_{d,q}}{D_{d,q}} - \int_q [g^2 \chi_{iC}(k-q)] \frac{W_{d,q}}{D_{d,q}}. \end{aligned} \quad (\text{C13})$$

Therefore, in the charge channel, real CDW fluctuations promote interband pairing attraction $V_{df} \propto -g^2 \chi_C$, whereas imaginary CDW fluctuations promote repulsion $V_{df} \propto g^2 \chi_{iC}$.

[1] K. Ishida, Y. Nakai, and H. Hosono, *J. Phys. Soc. Jpn.* **78**, 062001 (2009); D. C. Johnston, *Adv. Phys.* **59**, 803 (2010); J. Paglione and R. L. Greene, *Nat. Phys.* **6**, 645 (2010); P. C. Canfield and

S. L. Bud'ko, *Annu. Rev. Cond. Mat. Phys.* **1**, 27 (2010); H. H. Wen and S. Li, *ibid.* **2**, 121 (2011).
[2] P. Dai, J. Hu, and E. Dagotto, *Nat. Phys.* **8**, 709 (2012).

- [3] C. Fang, H. Yao, W.-F. Tsai, J. P. Hu, and S. A. Kivelson, *Phys. Rev. B* **77**, 224509 (2008).
- [4] C. Xu, M. Muller, and S. Sachdev, *Phys. Rev. B* **78**, 020501(R) (2008).
- [5] M. D. Johannes and I. I. Mazin, *Phys. Rev. B* **79**, 220510(R) (2009).
- [6] I. Eremin and A. V. Chubukov, *Phys. Rev. B* **81**, 024511 (2010).
- [7] E. Abrahams and Q. Si, *J. Phys.: Condens. Matter* **23**, 223201 (2011).
- [8] R. M. Fernandes, A. V. Chubukov, J. Knolle, I. Eremin, and J. Schmalian, *Phys. Rev. B* **85**, 024534 (2012).
- [9] S. Liang, A. Mukherjee, N. D. Patel, C. B. Bishop, E. Dagotto, and A. Moreo, *Phys. Rev. B* **90**, 184507 (2014).
- [10] L. Nie, G. Tarjus, and S. A. Kivelson, *Proc. Natl. Acad. Sci. USA* **111**, 7980 (2014).
- [11] R. M. Fernandes, A. V. Chubukov, and J. Schmalian, *Nat. Phys.* **10**, 97 (2014).
- [12] J.-H. Chu, J. G. Analytis, K. De Greve, P. L. McMahon, Z. Islam, Y. Yamamoto, and I. R. Fisher, *Science* **329**, 824 (2010).
- [13] T.-M. Chuang, M. P. Allan, J. Lee, Y. Xie, N. Ni, S. L. Bud'ko, G. S. Boebinger, P. C. Canfield, and J. C. Davis, *Science* **327**, 181 (2010).
- [14] M. Yi, D. Lu, J.-H. Chu, J. G. Analytis, A. P. Sorini, A. F. Kemper, B. Moritz, S.-K. Mo, R. G. Moore, M. Hashimoto, W. S. Lee, Z. Hussain, T. P. Devereaux, I. R. Fisher, and Z.-X. Shen, *Proc. Nat. Acad. Sci. USA* **108**, 6878 (2011).
- [15] J.-H. Chu, H.-H. Kuo, J. G. Analytis, and I. R. Fisher, *Science* **337**, 710 (2012).
- [16] S. Kasahara, H. J. Shi, K. Hashimoto, S. Tonegawa, Y. Mizukami, T. Shibauchi, K. Sugimoto, T. Fukuda, T. Terashima, A. H. Nevidomskyy, and Y. Matsuda, *Nature (London)* **486**, 382 (2012).
- [17] Y. Gallais, R. M. Fernandes, I. Paul, L. Chauviere, Y.-X. Yang, M.-A. Measson, M. Cazayous, A. Sacuto, D. Colson, and A. Forget, *Phys. Rev. Lett.* **111**, 267001 (2013).
- [18] X. Lu, J. T. Park, R. Zhang, H. Luo, A. H. Nevidomskyy, Q. Si, and P. Dai, *Science* **345**, 657 (2014).
- [19] E. P. Rosenthal, E. F. Andrade, C. J. Arguello, R. M. Fernandes, L. Y. Xing, X. C. Wang, C. Q. Jin, A. J. Millis, and A. N. Pasupathy, *Nat. Phys.* **10**, 225 (2014).
- [20] C. C. Lee, W. G. Yin, and W. Ku, *Phys. Rev. Lett.* **103**, 267001 (2009).
- [21] R. Applegate, R. R. P. Singh, C.-C. Chen, and T. P. Devereaux, *Phys. Rev. B* **85**, 054411 (2012).
- [22] R. M. Fernandes and A. J. Millis, *Phys. Rev. Lett.* **111**, 127001 (2013).
- [23] S. Lederer, Y. Schattner, E. Berg, and S. A. Kivelson, *Phys. Rev. Lett.* **114**, 097001 (2015).
- [24] J. Kang, A. F. Kemper, and R. M. Fernandes, *Phys. Rev. Lett.* **113**, 217001 (2014).
- [25] M. G. Kim, A. Kreyssig, A. Thaler, D. K. Pratt, W. Tian, J. L. Zarestky, M. A. Green, S. L. Bud'ko, P. C. Canfield, R. J. McQueeney, and A. I. Goldman, *Phys. Rev. B* **82**, 220503(R) (2010).
- [26] S. Avci, O. Chmaissem, J. M. Allred, S. Rosenkranz, I. Eremin, A. V. Chubukov, D. E. Bulgariu, D. Y. Chung, M. G. Kanatzidis, J.-P. Castellan, J. A. Schlueter, H. Claus, D. D. Khalyavin, P. Manuel, A. Daoud-Aladine, and R. Osborn, *Nat. Comm.* **5**, 3845 (2014).
- [27] A. E. Böhmer, F. Hardy, L. Wang, T. Wolf, P. Schweiss, and C. Meingast, *Nat. Comm.* **6**, 7911 (2015).
- [28] X. Wang and R. M. Fernandes, *Phys. Rev. B* **89**, 144502 (2014).
- [29] X. Wang, J. Kang, and R. M. Fernandes, *Phys. Rev. B* **91**, 024401 (2015).
- [30] J. Kang, X. Wang, A. V. Chubukov, and R. M. Fernandes, *Phys. Rev. B* **91**, 121104(R) (2015).
- [31] M. N. Gastiasoro and B. M. Andersen, *Phys. Rev. B* **92**, 140506(R) (2015).
- [32] J. Lorenzana, G. Seibold, C. Ortix, and M. Grilli, *Phys. Rev. Lett.* **101**, 186402 (2008).
- [33] G. Giovannetti, C. Ortix, M. Marsman, M. Capone, J. Brink, and J. Lorenzana, *Nat. Comm.* **2**, 398 (2011).
- [34] P. M. R. Brydon, J. Schmiedt, and C. Timm, *Phys. Rev. B* **84**, 214510 (2011).
- [35] G.-W. Chern, R. M. Fernandes, R. Nandkishore, and A. V. Chubukov, *Phys. Rev. B* **86**, 115443 (2012).
- [36] S. Chakravarty, R. B. Laughlin, D. K. Morr, and C. Nayak, *Phys. Rev. B* **63**, 094503 (2001).
- [37] C.-H. Hsu and S. Chakravarty, *Phys. Rev. B* **90**, 134507 (2014).
- [38] P. Chandra, P. Coleman, and A. I. Larkin, *Phys. Rev. Lett.* **64**, 88 (1990).
- [39] E. Berg, S. A. Kivelson, and D. J. Scalapino, *Phys. Rev. B* **81**, 172504 (2010).
- [40] Y. Kamiya, N. Kawashima, and C. D. Batista, *Phys. Rev. B* **84**, 214429 (2011).
- [41] Note that, in contrast to the stripe and CSDW phases, which are collinear and display a residual $O(2)$ symmetry, the noncollinear SVC phase breaks completely the spin-rotational symmetry.
- [42] K. A. Al-Hassanieh, C. D. Batista, G. Ortiz, and L. N. Bulaevskii, *Phys. Rev. Lett.* **103**, 216402 (2009).
- [43] Strictly speaking, the SVDW phase retains a mirror symmetry, and is therefore not chiral. Instead, the SVDW phase breaks inversion symmetry. We will nevertheless use the term “chiral” to describe it, as it captures the “handedness” of the spins around a plaquette.
- [44] S. Onoda and N. Nagaosa, *Phys. Rev. Lett.* **99**, 027206 (2007).
- [45] K. Matan, R. Morinaga, K. Iida, and T. J. Sato, *Phys. Rev. B* **79**, 054526 (2009).
- [46] H. Luo, M. Wang, C. Zhang, X. Lu, L.-P. Regnault, R. Zhang, S. Li, J. Hu, and P. Dai, *Phys. Rev. Lett.* **111**, 107006 (2013).
- [47] G. S. Tucker, R. M. Fernandes, D. K. Pratt, A. Thaler, N. Ni, K. Marty, A. D. Christianson, M. D. Lumsden, B. C. Sales, A. S. Sefat, S. L. Bud'ko, P. C. Canfield, A. Kreyssig, A. I. Goldman, and R. J. McQueeney, *Phys. Rev. B* **89**, 180503(R) (2014).
- [48] M. H. Christensen, Jian Kang, B. M. Andersen, I. Eremin, and R. M. Fernandes, *Phys. Rev. B* **92**, 214509 (2015).
- [49] S. E. Korshunov, *Phys. Rev. Lett.* **88**, 167007 (2002).
- [50] M. Hasenbusch, A. Pelissetto, and E. Vicari, *J. Stat. Mech.* (2005) P12002.
- [51] P. J. Hirschfeld, M. M. Korshunov, and I. I. Mazin, *Rep. Prog. Phys.* **74**, 124508 (2011); A. V. Chubukov, *Annu. Rev. Cond. Mat. Phys.* **3**, 57 (2012).
- [52] J. M. Allred *et al.*, [arXiv:1505.06175](https://arxiv.org/abs/1505.06175) [cond-mat.str-el].
- [53] B. P. P. Mallett, Yu. G. Pashkevich, A. Gusev, Th. Wolf, and C. Bernhard, *Europhys. Lett.* **111**, 57001 (2015).
- [54] S. Fujimoto, *Phys. Rev. Lett.* **106**, 196407 (2011).
- [55] H.-H. Kung, R. E. Baumbach, E. D. Bauer, V. K. Thorsmølle, W.-L. Zhang, K. Haule, J. A. Mydosh, and G. Blumberg, *Science* **347**, 1339 (2015).